Journal of Solid State Chemistry 183 (2010) 2552–2557

Contents lists available at ScienceDirect

Journal of Solid State Chemistry

journal homepage: www.elsevier.com/locate/jssc

Facile solvothermal synthesis of graphene–MnOOH nanocomposites

Sheng Chen [a], Junwu Zhu [a,*], Huajie Huang [a], Guiyu Zeng [b], Fude Nie [b], Xin Wang [a,*]

[a] Key Laboratory of Soft Chemistry and Functional Materials, Nanjing University of Science and Technology, Ministry of Education, Nanjing 210094, China
[b] Institute of Chemical Materials, China Academy of Engineering Physics, Mianyang 621900, China

ARTICLE INFO

Article history:
Received 1 May 2010
Received in revised form
9 August 2010
Accepted 18 August 2010
Available online 15 September 2010

Keywords:
Graphene
MnOOH
Nanocomposites
Solvothermal route
Catalysis

ABSTRACT

In this paper, we report a facile solvothermal route capable of aligning MnOOH nanocrystals on graphene. X-ray diffraction (XRD) and transmission electron microscopy (TEM) observations indicate that the exfoliated graphene sheets are decorated randomly by MnOOH nanocrystals, forming well-dispersed graphene–MnOOH nanocomposites. Dissolution-crystallization and oriented attachment are speculated to be the vital mechanisms in the synthetic process. The attachment of additives, such as MnOOH nanoparticles, are found to be beneficial for the exfoliation of GO as well as preventing the restack of graphene sheets. Moreover, cyclic voltammetry (CV) analyses suggest that the electrochemical reversibility is improved by anchoring MnOOH on graphene. Notably, the as-fabricated nanocomposites reveal unusual catalytic performance for the thermal decomposition of ammonium perchlorate (AP) due to the concerted effects of graphene and MnOOH. This template-free method is easy to reproduce, and the process proceeds at a low temperature and can be readily extended to prepare other graphene-based nanocomposites.

1. Introduction

Graphene, a monolayer of carbon atoms arranged in a honeycomb lattice, has attracted enormous attention in recent years from both the experimental and theoretical scientific communities [1–4]. Graphene oxide (GO) is one of the most important derivatives of graphene, which is a layered material bearing oxygen functional groups on their basal planes and edges [5–8]. Because of the special surface properties and layered structure, they become potential nanoscale building blocks for new materials [9–13]. Recent studies have shown that deposition of inorganic nanoparticles, such as Au, Pt, Cu_2O, ZnO, etc., onto graphene or GO sheets reveals special features in new hybrids and the nanocomposites have potential applications in catalysis, fuel cells, UV–vis absorption, lithium ion batteries, etc. [10,14–17].

Manganese oxyhydroxide (MnOOH) is a stable polymorph of trivalent hydroxide under ambient conditions, which is of considerable interest in many chemical processes including catalysis, molecular adsorption, model simulation, lithium ion batteries and so on [18–21]. Up to now, different nanostructures of MnOOH, such as nanorods and nano-branches, have been fabricated via a variety of methods [22,23]. Taking into account the fact that graphene, being unrolled carbon nanotubes (CNTs), possesses a high specific area (theoretically 2630 $m^2 g^{-1}$) and can serve as a superior platform for building nanocomposites. The combination of MnOOH and graphene may result in synergistic performances, supplying the nanocomposite with enhanced properties. However, there has been little research concerning the deposition of transition-metal oxyhydroxides, such as MnOOH nanocrystals, onto graphene sheets.

Herein, to broaden the horizon of using graphene as nanoscale building blocks for new hybrids, a two-step solvothermal procedure to synthesize graphene–MnOOH nanocomposites was developed. Graphene has shown an enhancement effect for MnOOH on both electrochemical and catalytic performances. This method is easy and straightforward, therefore can be readily extended as a general procedure to the preparation of other graphene-based nanocomposites.

2. Material and methods

2.1. Preparation

GO was prepared from powdered flake graphite (400 mesh) by a modified Hummers method as described previously [24,25]. Typically, two steps are involved in the whole procedure (Fig. 1). For the first step, 66.5 mg of GO and 0.36 g of $MnCl_2 \cdot 4H_2O$ were suspended in 30 mL of isopropanol with ultrasonication for ~30 min. The resulting homogeneous dispersion was then mixed with $KMnO_4$ solution (0.20 g of $KMnO_4$ dissolved in 5 mL De-ionized water) and stirred for about 15 min. Subsequently, the

* Corresponding authors. Fax: +86 25 8431 5054.
E-mail addresses: zhujw@mail.njust.edu.cn (J. Zhu), wxin@public1.ptt.js.cn (X. Wang).

0022-4596/$ - see front matter © 2010 Elsevier Inc. All rights reserved.
doi:10.1016/j.jssc.2010.08.026

slurry was loaded into a Teflon-lined stainless steel autoclave and heated at 120 °C for 12 h. After being cooled to room temperature, the black precipitate was collected and washed with DI-water and ethanol three times.

Thereafter, for the second step, as-obtained precipitate was redispersed in 30 mL EG with vigorous stirring for 15 min. The mixture was then loaded into a Teflon-lined stainless steel autoclave and heated at 120 °C for 16 h. The products were finally collected and dried in air at 60 °C. For comparison, pure MnOOH and graphene were synthesized chemically via a similar procedure in the absence of GO or manganese precursors, respectively.

2.2. Characterization

Powder X-ray diffraction (XRD) analyses were performed on a Bruker D8 Advance diffractometer with Cu$K\alpha$ radiation ($\lambda \approx 1.54$ Å) to examine the crystalline phase structure. FT-IR spectra of KBr powder pressed pellets were recorded on a Bruker VECTOR 22 spectrometer. Morphologies of as-obtained products were observed on transmission electron microscope (TEM, JEOL JEM-2100). Thermogravimetric analyses (TGA) were performed on a TGA/SDTA851e thermogravimetric analyzer from 50 to 300 °C at a heating rate of 10 °C min^{-1} in nitrogen flow. Differential scanning calorimetry (DSC) analyses were recorded on a TA-DSC-Q20 from 100 to 500 °C at a heating rate of 10 °C min^{-1} under nitrogen flow.

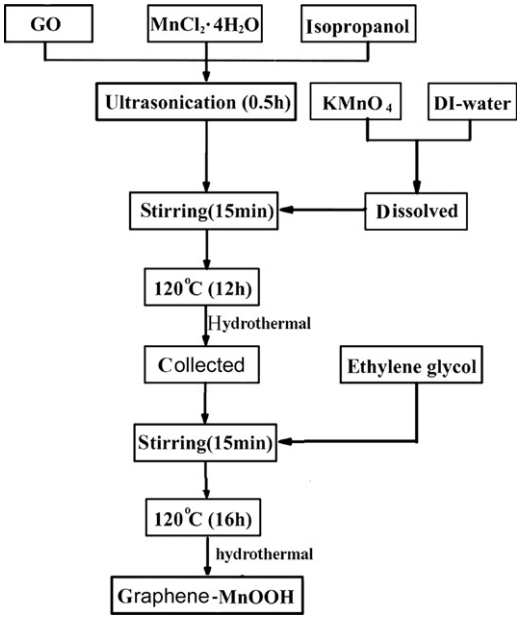

Fig. 1. Preparation procedure of graphene–MnOOH nanocomposites.

The electrochemical properties of as-obtained products were investigated under a three-electrode cell configuration at room temperature. Platinum foil and a saturated calomel electrode (SCE) were used as the counter and reference electrodes, respectively. The working electrodes were fabricated by mixing the prepared powders with 15 wt% acetylene black and 5 wt% polytetrafluorene-ethylene (PTFE) binder. A small amount of DI-water was added to the mixture to produce a homogeneous paste. The mixture was pressed onto nickel foam current-collectors (1.0×1.0 cm^2) to make electrodes. The mass of active material ranges from 4.5 to 6.2 mg. Before the electrochemical test, the prepared electrode was soaked overnight in a 6 M KOH solution. All electrochemical measurements were conducted on a CHI 660B electrochemical workstation (Shanghai CH Instrument Company, China).

3. Results and discussion

Typical XRD patterns of as-synthesized products are shown in Fig. 2. The most intensive peak at around $2\theta = 10.2°$ corresponds to the (001) reflection of GO, and the interlayer spacing (0.87 nm) is much larger than that of pristine graphite (0.34 nm), due to the introduction of oxygen-containing functional groups on the graphite sheets[11]. It is worth noting that the diffraction pattern of graphene–MnOOH is very close to the monoclinic phase of pure MnOOH (JCPDS 74-1632), and both the reflection of layered GO (001) and bulk graphite (002, around 26°) disappear, suggesting the coexistence of both MnOOH and exfoliated GO or graphene in as-fabricated hybrids [10,11].

Furthermore, in order to examine the deoxygenation of GO by this procedure, a controlled experiment using only GO as a precursor and keeping other conditions unaltered was carried out. The FT-IR spectra of GO and graphene are shown in Fig. 2b. The typical absorptions of GO are C=O stretching vibration of carboxyl group (1720 cm^{-1}), O–H deformation vibration of tertiary C–OH group (1398 cm^{-1}), and C–O stretching vibration of epoxy group (1052 cm^{-1}). Compared to GO, the above absorptions of the reduced sample have disappeared, suggesting the elimination of most of the oxygen-containing functional groups in the GO surfaces. The peak around 1616 cm^{-1} for the reduced sample can be assigned to the stretching vibrations of un-oxidized carbon backbone, consistenting with previous studies [8,26].

Heterostructure of as-prepared graphene–MnOOH nanocomposites are verified by TEM analyses (Fig. 3). It can be seen that graphene sheets are decorated randomly by MnOOH nanoparticles with diameters ranging from 20 to 80 nm. Lattice spacing of

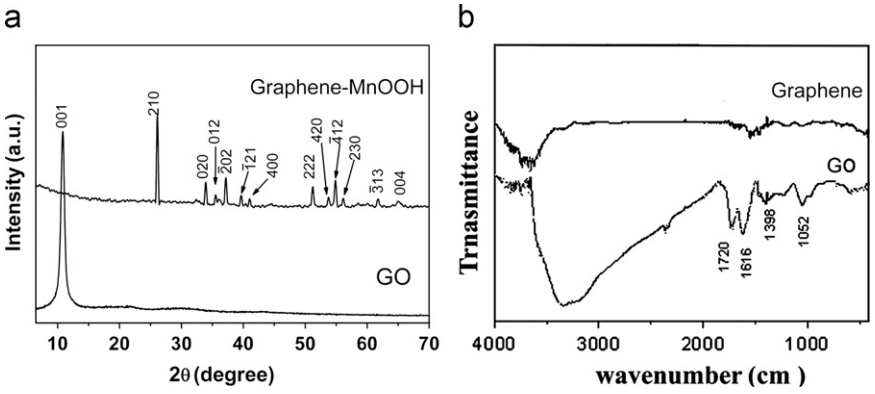

Fig. 2. (a) XRD patterns of GO and graphene–MnOOH and (b) FT-IR spectra of GO and graphene.

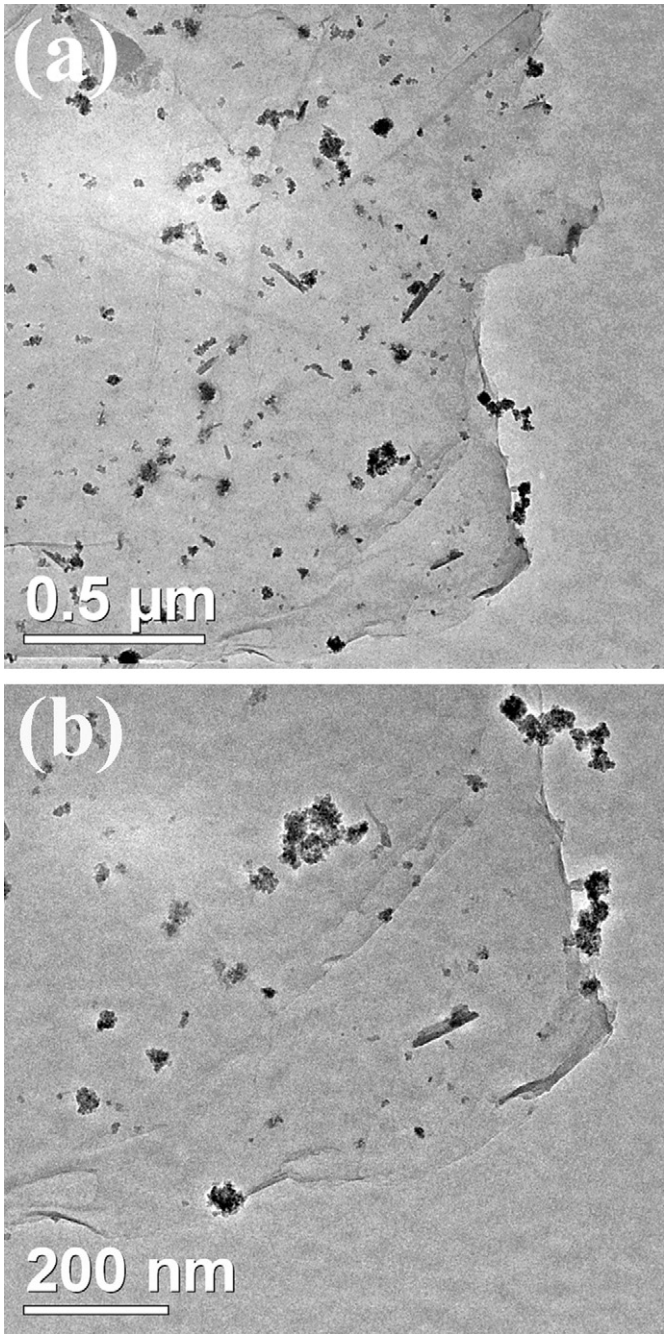

Fig. 3. TEM images of graphene–MnOOH nanocomposites.

approximately 0.52 and 0.33 nm corresponds to the distance between the (010) and (210) crystal planes of MnOOH, respectively (Fig. 1S, Supporting information).

Furthermore, to get a better understanding of the formation process of as-obtained products, some samples of graphene–MnOOH nanocomposites were taken at different time intervals. Fig. 4(a)–(c) illustrates the TEM images of samples collected at the first step. As shown in Fig. 4(a), the pristine GO sheets are multilayered with diameters of about a few micrometers, while a small amount of nanorods growing from the nuclei is observed at time interval of 30 min. Notably, the sample obtained at a reaction time of 12 h was exfoliated GO sheets decorated by a variety of rod-like nanocrystals. XRD pattern and HRTEM observations verify the nature of the tetragonal phase of α-MnO_2 (JCPDS 44-0141) of these rods (not shown). Moreover, GO (001) reflections in the XRD patterns are absent, giving evidence that GOs have been exfoliated at this step. Therefore, it can be derived that the hybrids of MnO_2 nanocrystals anchoring on exfoliated GO sheets have been obtained in the first step of our procedure.

Generally, GOs are produced from oxidation of bulk graphite, which maintains the AB stacking of the layers of graphite. Because of the large amounts of hydroxyl, carboxyl, carbonyl and epoxy functional groups on their basal or edge planes, GOs are strongly hydrophilic and easily exfoliated in water and some solvents (such as NMP, DMF, etc.), which enable their high capacity to form stable colloidal dispersions in these solvents. However, along with the increment of hydrophilicity during the oxidation process, GOs may gradually lose their excellent electrical properties and eventually becomes electrically insulated because of the transformation of carbon atoms from a planar sp^2-hybridized geometry to a distorted sp^3-hybridized geometry. To recover electrical conductivity, eliminating most of the oxygen-containing functional groups of GOs to restore the aromatic graphene networks is necessary [6,10–12].

It should be mentioned that MnOOH is also an interesting trivalent hydroxide under ambient conditions, which exhibits outstanding properties that have wide applications ranging from catalysis to lithium ion batteries. Considering the large specific area of graphenes are excellent building blocks for nanocomposites, the combination of graphene and MnOOH results in novel properties of the nanocomposite that can be utilized in many fields, for example, as a catalyzer for thermal decomposition of AP.

Ethylene glycol (EG), a low cost solvent, is also an effective agent for reducing GOs. On the other hand, reduction of manganese oxides, like MnO_2, is a common approach for producing MnOOH nanocrystals. Taking into account the facile exfoliation nature of GOs in EG as well as the mild reducibility of EG for both GO and MnO_2, a subsequent step using EG as both solvent and reducing agent to fabricate graphene–MnOOH from GO–MnO_2 is carried out [10].

Fig. 4(d)–(f) describes the whole reduction process of GO–MnO_2 to produce graphene–MnOOH nanocomposites. As recently demonstrated, graphenes can be obtained in bulk quantity by chemical reduction of GOs. However, the as-reduced graphene sheets tend to form irreversible agglomerates owning to the van der Waals interactions. Attaching molecules, such as MnOOH nanocrystals, onto the sheets is a feasible way to avoid aggregation and thus obtain graphene as individual sheets. In this step, with the reaction time elongated from 10 min to 16 h, striking transformation of attached nanocrystals is observed in the morphology (from nanorods to nanoparticles), providing evidence that the dissolution-crystallization mechanism is responsible for the composite formation. Remarkably, the graphene sheets are exfoliated and cannot restack, therefore it is seen that the dissolution of MnO_2 nanorods and the crystallization of MnOOH nanocrystallites contribute to preventing the graphenes restacking.

On the basis of the experimental results, the formation process of graphene–MnOOH nanocomposites is illustrated in Fig. 5. Generally, two steps are involved in the whole procedure: (1) exfoliation of GO and the attachment of MnO_2 nanorods on its surface; (2) deoxygenation of GO with the dissolution of MnO_2 nanorods and crystallization of MnOOH.

Specifically, for the first step, pristine graphite is initially oxidized to GO via a modified Hummer's method, with the interlayer spacing increased due to the introduction of oxygen-containing functional groups. The negative charged groups of GO are then favorable to interaction with Mn^{2+} via the electrostatic force, which can act as the anchor sites for the growth of crystal

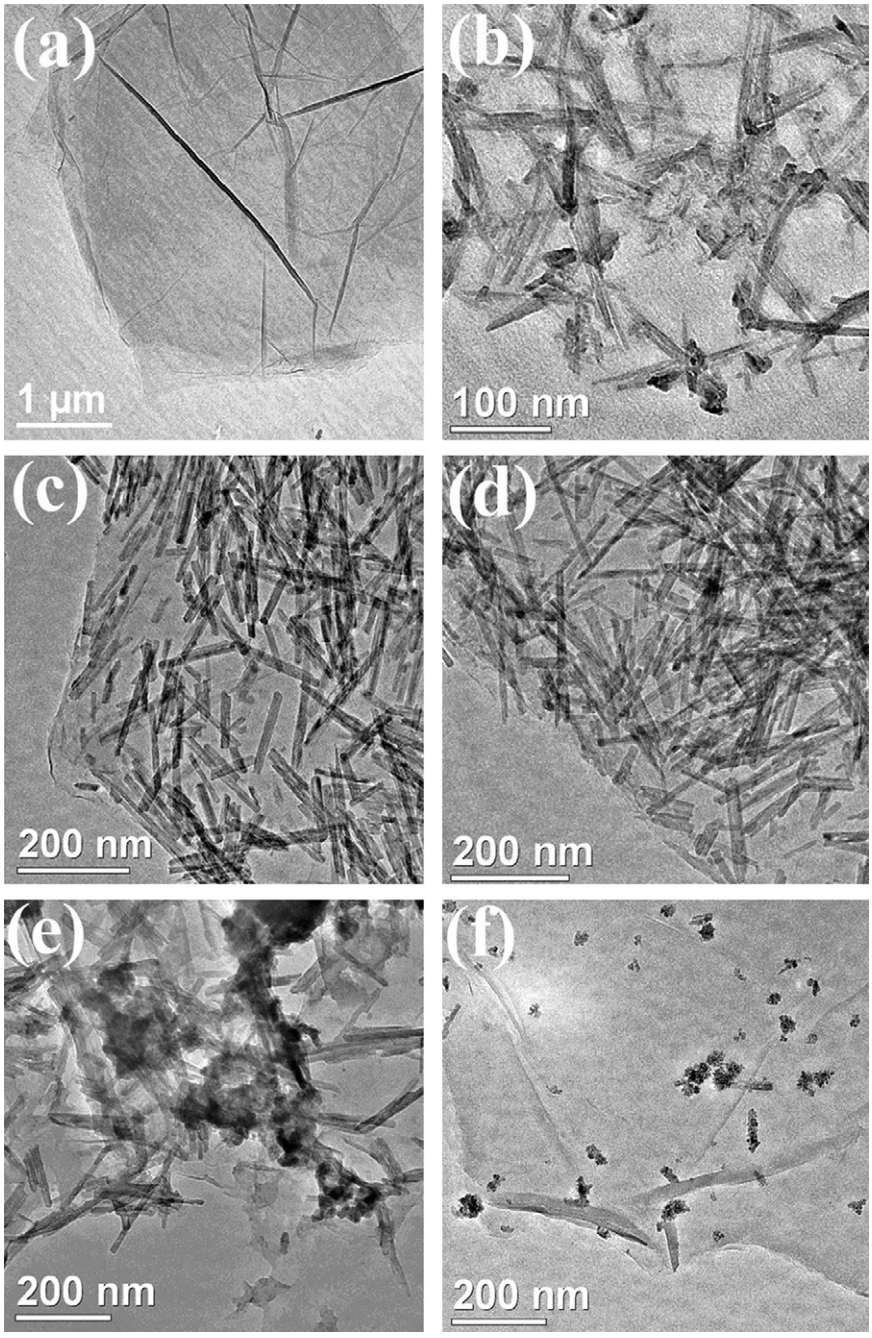

Fig. 4. TEM images of the intermediates of graphene–MnOOH nanocomposites collected at different time intervals: in the first step for the formation of GO-MnO_2 at (a) 0 min, (b) 30 min, (c) 12 h; in the second step for reducing GO–MnO_2 to form graphene–MnOOH at (e) 10 min, (f) 180 min, and (d) 16 h.

species. With the addition of $KMnO_4$ solution, a large amount of nuclei were produced from the redox reaction occurring between Mn^{2+} and MnO_4^- [27] and the crystal growth starts from the formation of nuclei. Because the (001) faces are the most favorable energetic ones and H_2O molecules coordinate with MnO_6 octahedron units more easily than isopropanol [28], with the addition of a small amount of water, only O atoms along the (001) direction of the MnO_6 units interact with H_2O, leaving those along other directions bound with isopropanol. Accordingly, the crystal species both thermodynamically and kinetically are favorable to grow along the (001) direction with low activation energy barriers, producing the primary nanorods with diameters of about 10 nm. Moreover, as discussed above, the oriented attachment thus should be another vital mechanism that is responsible for the lateral growth of MnO_2 nanorods [29].

To better understand the role of GO and graphene for the formation of highly dispersed MnOOH, MnOOH nanocrystals in the absence of GO was prepared and characterized by TEM (Fig. 2S, Supporting information). Comparing Fig. 4 with Fig. 2S, the MnO_2 nanorods on GO sheets show a lower length to diameter aspect ratio and with little aggregation in comparison with that in the absence of GO. When reaction time was elongated to 16 h, the highly dispersed MnOOH nanocrystals on graphene sheets with much smaller size in diameter could be obtained, in contrast, there were only MnOOH nanoparticle agglomerates for the graphene-free samples. Therefore, the GO and graphene sheets

can act as excellent dispersants. As will be discussed later, the high dispersibility will exert an influence on both electrochemical and catalytic behaviors of as-prepared products.

Fig. 5(b) and (c) illustrates the possible reactions for the synthesis of graphene–MnOOH at the second step. The weakening of graphene FT-IR adsorption in Fig. 2(b) implies most of the oxygen-containing functional groups have been removed, which is consistent with Rajamathi's descriptions [26]. XRD and TEM observations show that striking transformations on morphology and texture occur after solvothermal treatment with EG, which can be attributed to the redox reaction between MnO_2 and EG via a dissolution-recrystallization process. The whole process of the second step is proposed as follows: initially, the dissolved free Mn^{4+} ions are in equilibrium with MnO_2 in EG. With the solvothermal treatment at 120 °C, the redox reaction occurs between Mn^{4+} ions and EG. Since EG is in great excess, only one of the hydroxyl groups of EG is supposed to be oxidized to aldehyde or carboxyl groups, with Mn^{4+} simultaneously being reduced to Mn^{3+} [30]. The reactions then progresses slowly toward the right side as shown in Fig. 5(c), namely the rod-like MnO_2 nanocrystals dissolve in EG resulting in the reduction of Mn^{4+} at 120 °C, followed by the crystal growth of MnOOH. The concentration of Mn^{4+} is quite low due to the poor solubility of MnO_2 in EG, giving a lower supersaturation point for the growth of MnOOH crystallites. The dissolution-crystallization process continues for a long time (about 16 h, as indicated in Fig. 4(d)–(f)). Additionally, there are no other ions or surfactants, which might influence the growth direction through selective adsorption and desorption on crystal surfaces. The solution approach thus favors the full exposure of the surface of the crystal face, and MnOOH nuclei grow randomly in the reaction system, forming particulate shapes. Further study on the growth mechanism is still in progress.

Considering the good conductivity of graphene, and as mentioned above, MnOOH is a material with high electrochemical performance, anchoring of MnOOH nanocrystals on graphene sheets may lead to elevated electrochemical performances for the overall system. CV response of MnOOH, graphene, and graphene–MnOOH in 6 M KOH electrolyte is shown in Fig. 6. Two voltametric peaks are observed on the CV plots of MnOOH, corresponding to the redox reactions: $MnOOH+H_2O+e^- \leftrightarrow Mn(OH)_2+OH^-$. The nearly rectangular CV curve of graphene indicates the ideal capacitive nature of the fabricated electrode in strong alkaline electrolyte which is in accordance with previous reports [31]. Interestingly, when MnOOH nanocrystals are attached to the graphene sheets, the peaks at 0.315 and 0.035 V shift to 0.283 and 0.062 V, respectively. The separation between the two peak potentials can be used to determine the electrochemical reversibility for a redox couple, and the increasing value of separation indicates the presence of electrochemical irreversibility [32]. Accordingly, the reversibility for as-obtained graphene–MnOOH nanocomposites is improved.

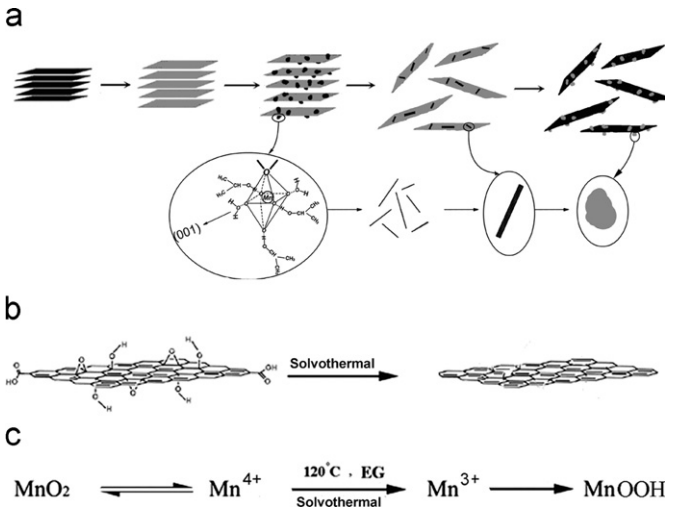

Fig. 5. (a) The formation process of graphene–MnOOH nanocomposites; (b) deoxygnation of GO to graphene via the solvothermal treatment; (c) dissolution of MnO_2 and crystallizaion of MnOOH.

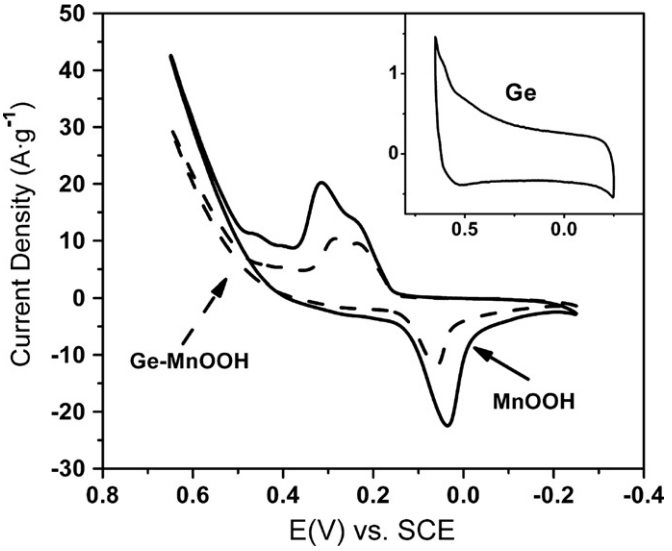

Fig. 6. CV curves of MnOOH, graphene, and graphene–MnOOH nanocomposites at 5 mV s^{-1} in 6 M KOH solution.

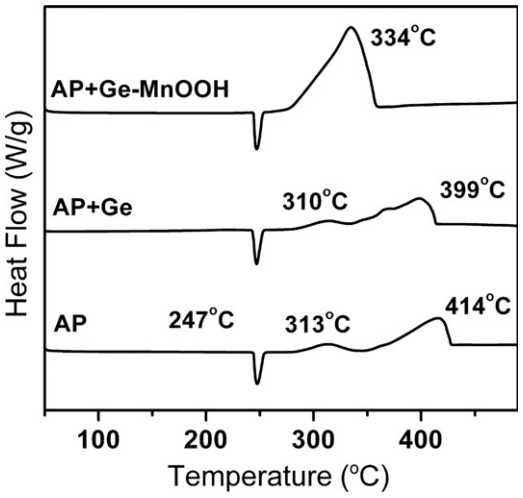

Fig. 7. DSC curves for the thermal decomposition of AP, AP with 2% graphene, and AP with 2% graphene–MnOOH nanocomposites.

To further explore potential applications, the catalysis of as-obtained graphene–MnOOH nanocomposite on the decomposition of AP was conducted. As displayed in Fig. 7, the thermal decomposition of pure AP show three events: the endothermic phase transition at 247 °C, the low-temperature decomposition (LTD) at 313 °C and the high-temperature decomposition (HTD) at 414 °C [33]. With the addition of 2% graphene into the system, the LTD and HTD decreased to 310 and 399 °C, respectively, due to the catalytic action of graphene. However, when graphene–MnOOH nanocomposites were added, the two steps (LTD and HTD) blended into one process at 334 °C with the exothermic heat (1392 J/g) much larger than that of net AP and AP–graphene

composites (590 and 540 J/g), revealing a good catalytic effect. According to previous studies, analogous to Fe_2O_3, MnOOH may promote the heterogeneous decomposition of deprotonized $HClO_4$ gas on the solid surface in the HTD, which reduces the temperature of the high temperature exothermic decomposition process without changing the low-temperature exothermic decomposition process very much [34–36]. Considering the large specific area of nanoscale MnOOH, which can provide more active sites, it exhibits high catalytic activity upon the decomposition of AP. But aggregation occurs when it is not dried in air, resulting in a decrement of the catalytic capability. In our procedure, the aggregation was inhibited to a certain extent by the decoration of MnOOH nanocrystals onto graphene sheets, giving higher catalytic performance. Although in the actual process the decomposition of AP would involve many additional steps, we believe these results calculated from the DSC measurements are still significant for material investigation.

Furthermore, the actual contents for each component in the as-synthesized samples were determined by TGA (Fig. 3S, supporting information). Part of the residual functional groups of graphene was decomposed while MnOOH was converted to manganese oxide. The ratios of weight loss for graphene, MnOOH, and graphene-MnOOH nanocomposites are found to be 13.4%, 6.0%, and 11.3%, respectively. The mass ratio of MnOOH/graphene was calculated to be a relatively low value of 0.28/1. Accordingly, there is a spacious room to improve the electrochemical or catalytic performances of the as-prepared composites.

4. Conclusions

In conclusion, graphene–MnOOH nanocomposites have been fabricated via a facile solvothermal procedure. The attachment of nanoparticles (MnO_2 and MnOOH nanocrystals) makes a great contribution to the exfoliation of GO as well as in preventing the restacking of graphene sheets. By decorating the graphene, the electrochemical reversible performance of MnOOH is enhanced. The obtained graphene-MnOOH nanocomposites show high catalytic activity on the thermal decomposition of AP. The as-synthesized products are also expected to have wide applications in ion exchange, separation, catalysis, and energy storage.

Acknowledgments

The authors are grateful for the financial support of the Natural Science Foundation of China, China Academy of Engineering Physics (nos. 10776014, 50902070), the Natural Science Foundation of Jiangsu(nos. BK2009391 and BE2009159), the Research Fund for the Doctoral Program of Higher Education of China (no. 20093219120011), and NUST Research Funding (NO.ZDJH07).

Appendix A. Supporting information

Supplementary data associated with this article can be found in the online version at doi:10.1016/j.jssc.2010.08.026.

References

[1] K.S. Novoselov, A.K. Geim, S.V. Morozov, D. Jiang, Y. Zhang, S.V. Dubonos, I.V. Grigorieva, A.A. Firsov, Science 306 (2004) 666–669.
[2] J. Wu, W. Pisula, K. Mullen, Chem. Rev. 107 (2007) 718–747.
[3] A.K. Geim, K.S. Novoselov, Nat. Mater. 6 (2007) 183–191.
[4] M. Lotya, Y. Hernandez, P.J. King, R.J. Smith, V. Nicolosi, L.S. Karlsson, F.M. Blighe, S. De, Z. Wang, I.T. McGovern, G.S. Duesberg, J.N. Coleman, J. Am. Chem. Soc. 131 (2009) 3611–3620.
[5] H. He, J. Klinowski, M. Forster, A. Lerf, Chem. Phys. Lett. 287 (1998) 53–56.
[6] A. Lerf, H. He, M. Forster, J. Klinowski, J. Phys. Chem. B 102 (1998) 4477–4482.
[7] S. Stankovich, R.D. Piner, S.T. Nguyen, R.S. Ruoff, Carbon 44 (2006) 3342–3347.
[8] H.K. Jeong, Y.P. Lee, R.J.W.E. Lahaye, M.H. Park, K.H. An, I.J. Kim, C.W. Yang, C.Y. Park, R.S. Ruoff, Y.H. Lee, J. Am. Chem. Soc. 130 (2008) 1362–1366.
[9] S. Stankovich, D.A. Dikin, K.M. Kohlhaas, E.J. Zimney, E.A. Stach, R.D. Piner, S.T. Nguyen, R.S. Ruoff, Nature 442 (2006) 282–286.
[10] C. Xu, X. Wang, J. Zhu, J. Phys. Chem. C 112 (2008) 19841–19845.
[11] C. Xu, X. Wang, J. Zhu, X. Yang, L. Lu, J. Mater. Chem. 18 (2008) 5625–5629.
[12] D. Li, R.B. Kaner, Science 320 (2008) 1170–1171.
[13] S. Park, R.S. Ruoff, Nat. Nanotech. 4 (2009) 217–224.
[14] C. Xu, X. Wang, L. Yang, Y. Wu, J. Solid State Chem. 182 (2009) 2486–2490.
[15] R. Muszynski, B. Seger, P.V. Kamat, J. Phys. Chem. C 112 (2008) 5263–5266.
[16] N. Karousis, S.P. Economopoulos, E. Sarantopoulou, N. Tagmatarchis, Carbon 48 (2010) 854–860.
[17] J. Wu, X. Shen, L. Jiang, K. Wanga, K. Chen, Appl. Surf. Sci. 256 (2009) 2826–2830.
[18] V.Q. Chiu, J.G. Hering, Environ. Sci. Technol. 34 (2000) 2029–2034.
[19] C.-C. Hu, Y.-T. Wu, K.-H. Chang, Chem. Mater. 20 (2008) 2890–2894.
[20] C.S. McArdell, A.T. Stone, J. Tian, Environ. Sci. Technol. 32 (1998) 2923–2930.
[21] G.R. Williams, A.J. Norquist, D. O'Hare, Chem. Mater. 18 (2006) 3801–3807.
[22] D. Zheng, Z. Yin, W. Zhang, X. Tan, S. Sun, Cryst. Growth Des. 6 (2006) 1733–1735.
[23] Y. Zhang, Y. Liu, F. Guo, Y. Hu, X. Liu, Y. Qian, Solid State Commun. 134 (2005) 523–527.
[24] W.S. Hummers, R.E. Offeman, J. Am. Chem. Soc. 80 (1958) 1339–1339.
[25] N.I. Kovtyukhova, P.J. Ollivier, B.R. Martin, T.E. Mallouk, S.A. Chizhik, E.V. Buzaneva, A.D. Gorchinskiy, Chem. Mater. 11 (1999) 771–778.
[26] C. Nethravathi, M. Rajamathi, Carbon 46 (2008) 1994–1998.
[27] M. Xu, L. Kong, W. Zhou, H. Li, J. Phys. Chem. C 111 (2007) 19141–19147.
[28] S. Chen, J. Zhu, Q. Han, Z. Zheng, Y. Yang, X. Wang, Cryst. Growth Des. 9 (2009) 4356–4361.
[29] D. Portehault, S. Cassaignon, E. Baudrin, J.P. Jolivet, Chem. Mater. 19 (2007) 5410–5417.
[30] V. Subramanian, H. Zhu, B. Wei, Chem. Phys. Lett. 453 (2008) 242–249.
[31] M.D. Stoller, S. Park, Y. Zhu, J. An, R.S. Ruoff, Nano Lett. 8 (2008) 3498–3502.
[32] R.S. Nicholson, Anal. Chem. 37 (1965) 1351–1355.
[33] Y. Wang, J. Zhu, X. Yang, L. Lui, X. Wang, Thermochim. Acta 437 (2005) 106–109.
[34] Y. Xu, D. Chen, X. Jiao, K. Xue, Mater. Res. Bull. 42 (2007) 1723–1731.
[35] H. Xu, X. Wang, L. Zhang, Powder Technol. 185 (2008) 176–180.
[36] V.V. Boldyrev, Thermochim. Acta 443 (2006) 1–36.